A Peridynamic Approach to Calculate the Elastoplastic Stress and Strain Fields

Átila L. Cruz[1], Mauricio V. Donadon[2]

[1]*Mechanics Division, Institute of Aeronautics and Space*
Praça Marechal Eduardo Gomes, 50, Vila das Acácias, 12228-904, São José dos Campos, São Paulo, Brazil
atila.lc@hotmail.com
[2]*Department of Aeronautical Engineering, Technological Institute of Aeronautics*
Praça Marechal Eduardo Gomes, 50, Vila das Acácias, 12228-900, São José dos Campos, São Paulo, Brazil
donadon@ita.br

Abstract. The peridynamic theory is a new approach developed in recent years for the numerical solution of elastodynamics problems. One of the advantages of the peridynamic theory is the natural capacity to simulate the initiation and growth of cracks in solid materials, without the aid of numerical procedures commonly employed in the conventional finite element formulation. This advantage is due to the peridynamic constitutive relations are based on partial integral equations, rather than differential ones, where these equations keep definite even with a geometrical discontinuity. This theory relies on the displacement fields of a given simulated problem, where the stress and strain fields are not obtained natively. Within this context, a numerical approach to calculate the strain and stress fields for a peridynamic elastoplastic simulation is presented, based on the developments published in the literature. The accuracy of this approach is verified by comparing the results for the Von Mises stress field obtained with the peridynamic theory, to those obtained with a commercial finite element code, and conclusions are drawn.

Keywords: peridynamic, stress analysis, elastoplastic simulations, plates with discontinuities.

1 Introduction

The peridynamic theory is a theory of continuum mechanics employed to solve complex engineering problems. With recent advancements in computational resources, it has become a popular powerful tool to simulate problems with discontinuities without additional numerical procedures, as commonly used in finite elements formulations (Sarego et al. [1]). This advantage is due to its constitutive relations being based on partial integral equations, rather than differential ones, where these relations continue to be valid on geometrical discontinuities (Bobaru et al. [2]).

For a peridynamic analysis, the simulated problem is divided into small volumes of material, represented by a single point, where each point interacts only with other points within a maximum distance, defined as horizon (Bobaru et al. [2]). This horizon must be defined carefully (Madenci and Oterkus [3]) because a small value can influence the direction of the crack growth, while a large value can cause an excessive wave dispersion and an increased computational cost without great gains in accuracy (Bobaru et al. [2]).

In a numerical simulation, the peridynamic theory only needs to calculate the force density between points and the displacement fields. However, in some elastodynamic problems, the stress-strain fields are also needed to better evaluate the solution. Some methods to calculate the stress fields with the peridynamic constitutive equations are shown in the literature, but these methods can only be used in problems with homogeneous bodies and uniform deformations (Bobaru et al. [2]), or for local problems (Madenci and Oterkus [3]).

To overcome these problems, a new method based on the peridynamics was published (Madenci et al. [4], Madenci et al. [5], and Madenci et al. [6]). This new method, called peridynamic differential operators, uses its

peridynamic numerical framework to obtain the derivative of a given field using partial integral functions.

Within this context, this research aims to verify the applicability of these operators to compute an elastoplastic stress-strain field. To verify this approach, these peridynamic operators are implemented into an in-house elastoplastic peridynamic FORTRAN code, and the results obtained are compared to the available analytical results and those obtained with a commercial finite element code.

2 The peridynamic theory

The peridynamic elastoplastic constitutive model used in this paper is developed by Madenci and Oterkus [7]. This constitutive model has some limitations, as small strains and infinitesimal rotations (Le and Bobaru [8]), but was chosen due to its well-developed plasticity correction procedure with isotropic hardening. For the domain shown in Fig. 1, the points are spaced by a distance Δ and each one represents a small volume V.

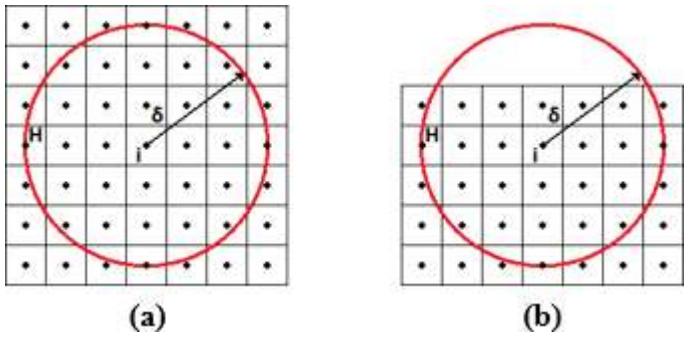

Figure 1. The family of point i: (a) complete neighborhood and (b) incomplete neighborhood

For point i, the center of a region called neighborhood H, defined in this paper by a distance (horizon) δ=3Δ, the equation of motion is shown in eq. (1) (Bobaru et al. [2]). In this equation, ρ_i is the mass density, $\ddot{\mathbf{u}}$ is the acceleration and **b** is the body force density vector, υ is the volume correction factor (Madenci and Oterkus [3]), while the subscript j represents the other points inside H besides i.

$$\rho_i \ddot{\boldsymbol{u}} = \sum_{j \in H} (\boldsymbol{t}_{ij} - \boldsymbol{t}_{ji}) \upsilon_j V_j + \boldsymbol{b}_i. \tag{1}$$

For a bond between points i and j, the force state is defined in eq. (2) (Madenci and Oterkus [7]), where b, d (Madenci and Oterkus [7]), a_k and a_G (Pashazad and Kharazi [9]) are the peridynamic materials parameters, while **x** and **y** are the distance vector in the non-deformed and deformed configuration. The parameter G_{ij} is the surface correction factor (Madenci and Oterkus [3]), needed for incomplete neighborhoods (see Fig. 1).

$$\boldsymbol{t}_{ij} = \left[(a_k - a_G) 2\delta d \frac{\Lambda_{ij}}{|\boldsymbol{x}_j - \boldsymbol{x}_i|} \theta_i^e + 2\delta b s_{ij}^e \right] G_{ij} \frac{\boldsymbol{y}_j - \boldsymbol{y}_i}{|\boldsymbol{y}_j - \boldsymbol{y}_i|}. \tag{2}$$

The elastic dilatation θ_i^e, elastic stretch s_{ij}^e, and the parameter Λ_{ij} are obtained by eq. (3) (Madenci and Oterkus [7]).

$$\theta_i^e = d\delta \sum_{j \in H} s_{ij}^e \Lambda_{ij} G_{ij} \upsilon_j V_j \ , \quad s_{ij}^e = \frac{|\boldsymbol{x}_j - \boldsymbol{x}_i| - |\boldsymbol{y}_j - \boldsymbol{y}_i|}{|\boldsymbol{x}_j - \boldsymbol{x}_i|} - s_{ij}^{pl}, \quad \Lambda_{ij} = \frac{\boldsymbol{x}_j - \boldsymbol{x}_i}{|\boldsymbol{x}_j - \boldsymbol{x}_i|} \cdot \frac{\boldsymbol{y}_j - \boldsymbol{y}_i}{|\boldsymbol{y}_j - \boldsymbol{y}_i|}. \tag{3}$$

The plastic stretch s_{ij}^{pl} is calculated incrementally, as shown by Madenci and Oterkus [7] and by Pashazad and Kharazi [9]. His value is updated when the yield function F_i, in eq. (4), is greater than zero in a given time step n. In this function, the σ_0, E_t, and G are the original yield stress, the tangent modulus, and the shear modulus, respectively.

$$F_i = W_i^{G\,e} - G_i^p = \left[b\delta \sum_{j \in H} s_{ij}^{e\,2} |\boldsymbol{x}_j - \boldsymbol{x}_i| G_{ij} \upsilon_j V_j - a_G \theta_i^{e\,2} \right] - \left[\frac{\left(\sigma_0 + E_t s_i^{pl}\right)^2}{6G} \right]. \tag{4}$$

For a time step n, the value of the plastic stretch s_{ij}^{pl} is updated by eq. (5) (Pashazad and Kharazi [9]).

$$s_{ij}^{pl} = \left(s_{ij}^{pl}\right)^{n-1} + C_i B_{ij}\,, \quad B_{ij} = \left(s_{ij}^{e}\right)^{n-1}\left|\boldsymbol{x}_j - \boldsymbol{x}_i\right|. \tag{5}$$

Likewise, the equivalent plastic stretch s_i^{pl} is calculated by eq. (6), where A_0 is another peridynamic material parameter (Madenci and Oterkus [7]).

$$s_i^{pl} = \left(s_i^{pl}\right)^{n-1} + C_i A_0 \sqrt{b\delta \sum_{j\in H} B_{ij}^2 \left|\boldsymbol{x}_j - \boldsymbol{x}_i\right| G_{ij} v_j V_j}. \tag{6}$$

In Madenci and Oterkus [7] and Pashazad and Kharazi [9], the value of C_i is obtained using the Newton-Raphson iterative method on the yield function. However, another approach is proposed here to simplify these calculations. Reorganizing the yield function with eq. (5), eq. (6), and leaving C_i in evidence, this equation is then simplified to the quadratic polynomial in eq. (7). The value of C_i is defined as its lowest root, to agree with the iterative method using a zero seed.

$$\begin{aligned} F_i = C_i^2 & \begin{bmatrix} b\delta \sum_{j\in H} B_{ij}^2 \left|\boldsymbol{x}_j - \boldsymbol{x}_i\right| G_{ij} v_j V_j \\ -a_G \left(d\delta \sum_{j\in H} B_{ij} \Lambda_{ij} G_{ij} v_j V_j \right)^2 - \dfrac{\left(E_t A_0 \sqrt{b\delta \sum_{j\in H} B_{ij}^2 \left|\boldsymbol{x}_j - \boldsymbol{x}_i\right| G_{ij} v_j V_j} \right)^2}{6G} \end{bmatrix} \\ + C_i & \begin{Bmatrix} 2a_G d\delta (\theta_i^e)^{n-1} \sum_{j\in H} B_{ij} \Lambda_{ij} G_{ij} v_j V_j \\ -2b\delta \sum_{j\in H} B_{ij}^2 G_{ij} v_j V_j - \dfrac{E_t A_0 \sqrt{b\delta \sum_{j\in H} B_{ij}^2 \left|\boldsymbol{x}_j - \boldsymbol{x}_i\right| G_{ij} v_j V_j} \left[\sigma_0 + E_t \left(s_i^{pl}\right)^{n-1}\right]}{3G} \end{Bmatrix} \\ & + \left\{ b\delta \sum_{j\in H} B_{ij} \left(s_{ij}^e\right)^{n-1} G_{ij} v_j V_j - a_G \left(\theta_i^{e2}\right)^{n-1} - \frac{\left[\sigma_0 + E_t \left(s_i^{pl}\right)^{n-1}\right]^2}{6G} \right\}. \end{aligned} \tag{7}$$

3 Stress-strain fields calculation for a plane stress analysis

To calculate the strain fields **ε**, the partial derivative of the displacement fields **u** must be first obtained, where these derivatives are obtained in this paper using the peridynamic differential operators. The first partial derivatives for a 2D analysis could be approximated by eq. (8) (Madenci et al. [5]).

$$\begin{Bmatrix} u_{,x} \\ u_{,y} \end{Bmatrix} = \sum_{j\in H} \left(\boldsymbol{u}_j - \boldsymbol{u}_i\right) \begin{Bmatrix} g_2^{10} \\ g_2^{01} \end{Bmatrix} V_j. \tag{8}$$

The peridynamic operators g_2^{10} and g_2^{01} are obtained in eq. (9) (Madenci et al. [5] with Madenci et al. [6]), where ξ_x and ξ_y are the components of the distance vector **x** on the X and Y ordinate directions, respectively.

$$\begin{Bmatrix} g_2^{10} \\ g_2^{01} \end{Bmatrix} = \left(\frac{\delta}{\left|\boldsymbol{x}_j - \boldsymbol{x}_i\right|}\right)^2 \left[\begin{Bmatrix} a_{10}^{10} \\ a_{10}^{01} \end{Bmatrix} \xi_x + \begin{Bmatrix} a_{01}^{10} \\ a_{01}^{01} \end{Bmatrix} \xi_y + \begin{Bmatrix} a_{20}^{10} \\ a_{20}^{01} \end{Bmatrix} \xi_x^2 + \begin{Bmatrix} a_{02}^{10} \\ a_{02}^{01} \end{Bmatrix} \xi_y^2 + \begin{Bmatrix} a_{11}^{10} \\ a_{11}^{01} \end{Bmatrix} \xi_x \xi_y \right]. \tag{9}$$

The parameters "a" in eq. (9) are obtained by solving a linear system for every point i. If a neighborhood has the same point distribution as another, is verified that the peridynamic operators will be the same. The matrix and vectors for the linear system [A].{a}={b} are listed in eq. (10) (Madenci et al. [6]).

$$A = \sum_{j\in H} \left(\frac{\delta}{\left|\boldsymbol{x}_j - \boldsymbol{x}_i\right|}\right)^2 \begin{bmatrix} \xi_x^2 & \xi_x\xi_y & \xi_x^3 & \xi_x\xi_y^2 & \xi_x^2\xi_y \\ & \xi_y^2 & \xi_x^2\xi_y & \xi_y^3 & \xi_x\xi_y^2 \\ & & \xi_x^4 & \xi_x^2\xi_y^2 & \xi_x^3\xi_y \\ & sym & & \xi_y^4 & \xi_x\xi_y^3 \\ & & & & \xi_x^2\xi_y^2 \end{bmatrix} V_j\,, \quad a = \begin{bmatrix} a_{10}^{10} & a_{10}^{01} \\ a_{01}^{10} & a_{01}^{01} \\ a_{20}^{10} & a_{20}^{01} \\ a_{02}^{10} & a_{02}^{01} \\ a_{11}^{10} & a_{11}^{01} \end{bmatrix}, \quad b = \begin{bmatrix} 1 & 0 \\ 0 & 1 \\ 0 & 0 \\ 0 & 0 \\ 0 & 0 \end{bmatrix}. \tag{10}$$

With these displacement partial derivatives, the strain fields are then obtained in eq. (11) (Crisfield [10]), where the subscript x and y stand for X and Y ordinate direction, and ε_x, ε_y, and γ_{xy} are the strains in X, Y and XY directions respectively.

$$\varepsilon_x = u_{x,x}, \quad \varepsilon_y = u_{y,y}, \quad \gamma_{xy} = u_{x,y} + u_{y,x}. \tag{11}$$

The stress fields are obtained with an incremental approach in each time step n as shown in eq. (12), where [C] is the constitutive matrix and **σ** represents the stress fields (Crisfield [10]).

$$\begin{Bmatrix} \sigma_x \\ \sigma_y \\ \tau_{xy} \end{Bmatrix} = \begin{Bmatrix} \sigma_x \\ \sigma_y \\ \tau_{xy} \end{Bmatrix}^{n-1} + [C]\left(\begin{Bmatrix} \varepsilon_x \\ \varepsilon_y \\ \gamma_{xy} \end{Bmatrix} - \begin{Bmatrix} \varepsilon_x \\ \varepsilon_y \\ \gamma_{xy} \end{Bmatrix}^{n-1} \right). \tag{12}$$

When necessary, the plasticity correction procedure used on these stresses is obtained from the Prandtl-Reuss equations. This procedure is detailed in Crisfield [10].

4 Numerical simulations

All equations and definitions presented in Section 2 and Section 3 are implemented in an in-house Fortran code, based on a previous work developed by the authors (Cruz and Donadon [11]). In this code, the time integration scheme is the adaptive relaxation method (Oakley and Knight Jr [12]), with the stable time step calculated by the Courant-Friedrichs-Lewy approach (Bobaru et al. [2]).

The numerical simulations done in this paper involves two plates with discontinuity: one plate with a central crack and another with a central hole, loaded by displacement constraints on the regions indicated in Fig. 2. The displacements are enforced as a fictitious boundary layer, with a depth of 2δ, and are applied over a set amount of time steps to prevent abrupt loads in the simulation (Madenci and Oterkus [3]). Also, if any bond between points i and j crosses the crack, neither point belongs to the region H of the other point.

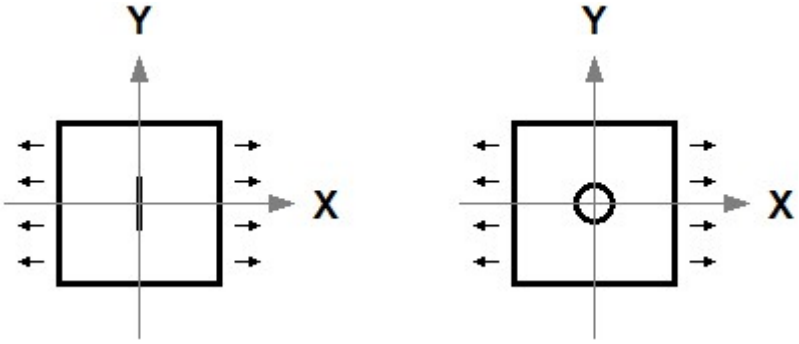

Figure 2. Simulated plates for the first plate

The dimensions and the material properties are listed in Tab. 1.

Table 1. Geometrical and material properties

Properties	Value
Edges	50 mm x 50 mm
Thickness (h)	1 mm
Distance between points (Δ)	0.16 mm
Length of crack (2a)	10 mm
Hole radius (r)	1 mm
Density (ρ)	2800 kg/m³
Poisson's ratio (ν)	0.33
Young's modulus (E)	71.71 GPa
Tangent modulus (E_t)	461.95 GPa
Yield stress (σ_y)	0.94 GPa

4.1 Verification of the implemented code for prediction of the stress distribution in an elastic plate with a hole and a plate with a central crack

This first test aims to verify if the implemented code concentrates stress in a pure elastic simulation around defects as expected in the literature. Both plates are loaded with a prescribed strain field of ε_x=3mm/m, ε_y=-$\nu\varepsilon_x$ and γ_{xy}=0, applied over 500 time increments on both ends, where the displacement constraints are then calculated with eq. (13). In this equation, u_x and u_y are the displacements and x_x and x_y are the position on the X and Y directions, respectively. For this test, the code's plasticity subroutine is disabled.

$$u_x = x_x\varepsilon_x\,, \quad u_y = x_y\varepsilon_y\,. \tag{13}$$

The analytical stress distribution on the X direction, from the tip of the crack towards its edge in the Y direction, is shown in eq. (14) (Tada et al. [13]), where σ_{x0} is the stress applied on the plate (calculated from the strain boundary conditions), *a* is the crack length and *z* is the distance from the crack tip.

$$\sigma_{x\,crack} = \frac{\sigma_{x0}}{\sqrt{1-(a/z)^2}}. \tag{14}$$

For a plate with a central hole the expression for the stress distribution along the Y direction is given by eq. (15) (Young and Budynas [14]), where *r* is the hole radius and *z* is the distance from the hole border.

$$\sigma_{x\,hole} = \frac{\sigma_{x0}}{2}\left(2+\frac{r^2}{z^2}+3\frac{r^4}{z^4}\right). \tag{15}$$

The stress distribution calculated by the Fortran code compared with the analytical solution for the two plates is presented in Fig. 3.

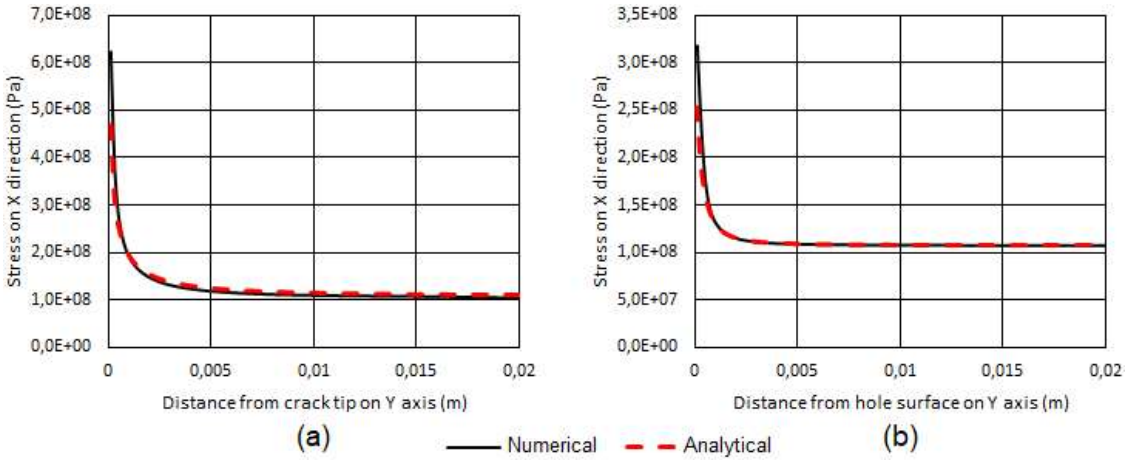

Figure 3. Stress distribution for a plate with a defect: (a) a central crack and (b) a central hole

As shown in Fig. 3, a very good correlation between numerical and analytical stress distribution was obtained. For the plate with a central hole, the stress intensity factor obtained in this test is k_t=2.95, which is very close to the analytical value k_t=3 (Young and Budynas [14]). For both plates with a central crack and a central hole, the stress distributions obtained in the simulation are very close to those calculated with the analytical solution, suggesting that the elastic response is accurately predicted by using the PD elastic formulation implemented into the in-house Fortran code.

4.2 Verification of the implemented code for elastoplastic simulations

This test aims to verify the accuracy of the peridynamic and classical elastoplastic formulations presented in Section 2 and Section 3. These accuracies are verified by comparing the Von Mises Stress Field obtained with the peridynamic theory to those obtained with a commercial finite element code (Abaqus).

In this test, the two plates are loaded with a displacement constraint of u_x=±0.125mm in the X direction and

u_y=0 in the Y direction on both ends, applied over 15000 time increments. For the Abaqus FE code, the crack is modeled as a notch with round tips with a diameter of 0.05mm. The geometries were discretized using the CPS3 element type available in the Abaqus FE elements library.

Running the simulations, the results for the plate with central crack are depicted in Fig. 4.

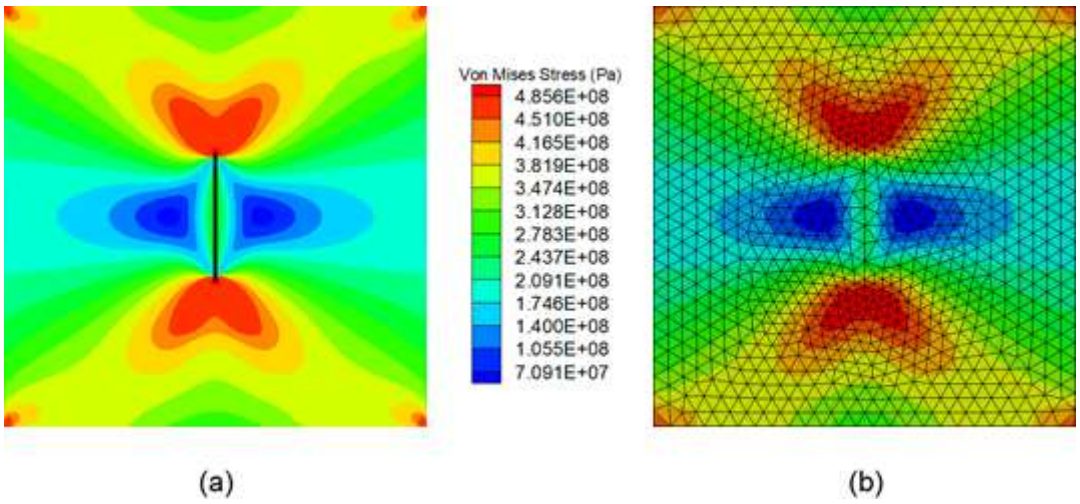

Figure 4. Von Mises stress field for a plate with central crack for: (a) implemented Fortran code (b) Abaqus

And the results for the plate with a central hole are depicted in Fig. 5.

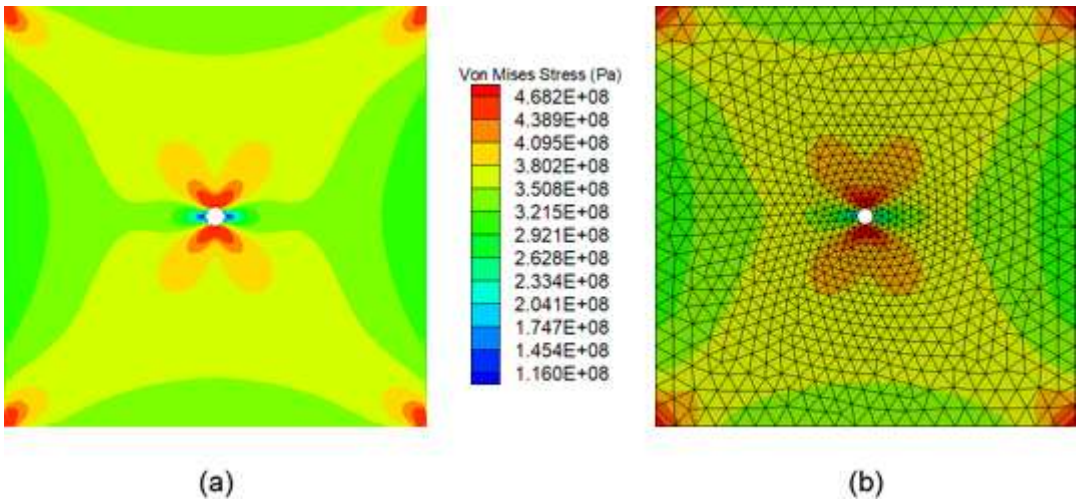

Figure 5. Von Mises stress field for a plate with central hole for: (a) implemented Fortran code (b) Abaqus

As shown in Fig. 4 and Fig. 5, the results obtained with the finite element approach were very close to those obtained with the peridynamic theory. These results show the reliability and accuracy of the proposed implemented approach to simulate an elastoplastic problem and the efficiency of the peridynamic differential operators.

5 Conclusions

This paper presented an approach to calculate the stress and strain fields for a peridynamic simulation using the peridynamic differential operators. These operators, while using their peridynamic framework to approximate the strain fields, do not have the drawbacks discussed in the literature when calculating this field using the peridynamic constitutive relations. The partial integral functions used remain valid even when a geometric discontinuity appears in the simulated problem, allowing the calculation of this field during the simulation.

The formulations were implemented into an in-house Fortran code under development by the authors, where some validation cases were presented. In general, a good correlation between numerical predictions obtained using the proposed model, analytical solutions, and FE results was obtained for several benchmark study cases available in the literature.

The first case verified the stress distribution on an elastic 2D plate with central discontinuities. The stress distribution calculated by the program was very close to the analytical solution presented in the literature, indicating that the methodology correctly predicts the stress and strain fields for non-uniform problems.

The second case verified the peridynamic and the classical plasticity correction method. The results for the three simulated plates were very close to the ones predicted with the commercial finite element code. These results indicate that the polynomial form of the yield function for the calculation of C_i proposed in eq. (7) was a good substitute to the Newton-Raphson iterative method proposed by Madenci and Oterkus [7] and by Pashazad and Kharazi [9].

Acknowledgements. This project is partially funded by CNPq, grant number 301069/2019-0.

Authorship statement. The authors hereby confirm that they are the sole liable persons responsible for the authorship of this work, and that all material that has been herein included as part of the present paper is either the property (and authorship) of the authors, or has the permission of the owners to be included here.

References

[1] G. Sarego, Q. V. Le, F. Bobaru, M. Zaccariotto and U. Galvanetto. "Linearized State-based Peridynamics for 2-D Problems". *International Journal for Numerical Methods in Engineering*, vol. 108, n. 10, pp. 1174-1197, 2016.
[2] F. Bobaru, J. T. Foster, P. H. Geubelle and S. A. Silling. *Advances in Applied Mathematics: Handbook of Peridynamic Modeling*. CRC Press, 2016.
[3] E. Madenci and E. Oterkus. *Peridynamic Theory and Its Applications*. Springer, 2014.
[4] E. Madenci, A. Barut and M. Futch. "Peridynamic differential operator and its applications". *Computer Methods in Applied Mechanics and Engineering*, vol. 304, pp. 408-451, 2016.
[5] E. Madenci, M. Dorduncu, A. Barut and M. Futch. "Numerical solution of linear and nonlinear partial differential equations using the peridynamic differential operator". *Numerical Methods for Partial Differential Equations*, vol. 33, n. 5, pp. 1726-1753, 2017.
[6] E. Madenci, A. Barut and M. Dorduncu. *Peridynamic Differential Operator for Numerical Analysis*. Springer, 2019.
[7] E. Madenci and S. Oterkus. "Ordinary State-based Peridynamics for Plastic Deformation According to Von Mises Yield Criteria with Isotropic Hardening". *Journal of the Mechanics and Physics of Solids*, vol. 86, pp. 192-219, 2016.
[8] Q. V. Le and F. Bobaru. "Objectivity of State-Based Peridynamic Models for Elasticity". *Journal of Elasticity*, vol. 131, n. 1, pp. 1-17, 2018.
[9] H. Pashazad and M. Kharazi. "A peridynamic plastic model based on von Mises criteria with isotropic, kinematic and mixed hardenings under cyclic loading". *International Journal of Mechanical Sciences*, vol. 156, pp. 182-204, 2019.
[10] M. A. Crisfield. *Non-linear Finite Element Analysis of Solids and Structures: Volume 1*. John Wiley & Sons, 1991.
[11] A. L. Cruz and M. V. Donadon. "Application of the Peridynamic Theory in the Stress Field Analysis of Plates with Geometric Discontinuities". In: *Proceedings of 7th International Symposium on Solid Mechanics* (Mecsol 2019).
[12] D. R. Oakley and N. F. Knight Jr. "Adaptive Dynamic Relaxation Algorithm for Non-linear Hyperelastic Structures: Part I Formulation". *Computer Methods in Applied Mechanics and Engineering*, vol. 126, n. 1-2, pp. 67-89, 1995.
[13] H. Tada, P. C. Paris and G. R. Irwin. *The Stress Analysis of Cracks Handbook: Third Edition*. ASME Press, 2000.
[14] W. C. Young and R. G. Budynas. *Roark's Formulas for Stress and Strain: Seventh Edition*. McGraw-Hill, 2002.